Engineering Fracture Mechanics 275 (2022) 108821

Contents lists available at ScienceDirect

Engineering Fracture Mechanics

journal homepage: www.elsevier.com/locate/engfracmech

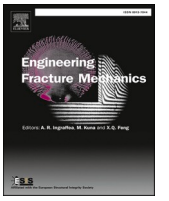

A fracture mechanics approach to the design of hybrid-reinforced concrete beams

Federico Accornero [a,*], Alessio Rubino [a], Alberto Carpinteri [a,b]

[a] Dept of Structural, Geotechnical and Building Engineering, Politecnico di Torino, Torino, Italy
[b] Zhujiang (Pearl River) Professor of Guangdong Province, Dept of Civil and Environmental Engineering, Shantou University, Shantou, PR China

ARTICLE INFO

Keywords:
Hybrid-reinforced concrete
Fracture mechanics
Updated Bridged Crack Model
Minimum reinforcement
Scale effects

ABSTRACT

The Updated Bridged Crack Model (UBCM) is proposed as a fracture mechanics tool to thoroughly predict the structural behaviour of hybrid-reinforced concrete (HRC) beams. The cementitious matrix is assumed to be linear-elastic perfectly-brittle, whereas nonlinear constitutive laws are used to describe the toughening action of the reinforcing phases, which is due to the yielding of steel-bars and to the pull-out of the short fibres.

Under these assumptions, the model predicts different HRC post-cracking structural behaviours that can be synthetically described by three scaling dimensionless numbers: the *bar-reinforcement brittleness number*, N_{P}, which is directly related to the steel-bar reinforcement percentage, ρ; the *fibre-reinforcement brittleness number*, $N_{\mathrm{P,f}}$, which depends on the fibre volume fraction, V_{f}; and the *pull-out brittleness number*, N_{w}, which is a function of the critical embedded length of the fibre-reinforcement, w_{c}. An effective relationship between the two reinforcement brittleness numbers is proved to define the minimum reinforcement conditions for HRC beams. All the other parameters being the same, it can be translated into a relationship between the steel-bar and the short-fibre reinforcement ratios, thus providing an effective and straightforward tool for the minimum reinforcement design of HRC structures.

1. Introduction

During the last forty years, an extensive research work has focused onto the beneficial influence of reinforcing fibres on the mechanical behaviour of cementitious composites. This is relevant either when the fibres represent a single reinforcing phase —i.e., in the case of fibre-reinforced concrete (FRC) elements [1–11]— or when they represent a supplementary reinforcement in addition to the traditional steel-bars, leading to the definition of the so-called *hybrid-reinforced concrete* (HRC) [12–22]. In both cases, it is widely acknowledged that the fibres provide an improvement of the mechanical properties of the composite, including fracture energy, as well as tensile, compressive, and shear strengths.

The main feature of fibre-reinforced composites is that their energy dissipation capacity dramatically changes depending on several factors, among which: (i) the fibre volume fraction, V_{f}; (ii) the mechanical and geometrical properties of the reinforcing fibres (tensile strength, geometric profile, and aspect ratio) and of the cementitious matrix (mainly, its compression strength) [23–26]; (iii) the specimen sizes [27–30]; (iv) the fibre distribution within the volume of the composite [31].

In the scientific literature, the constitutive law of fibre-reinforced cementitious composites is generally described by a single

* Corresponding author.
E-mail address: federico.accornero@polito.it (F. Accornero).

https://doi.org/10.1016/j.engfracmech.2022.108821
Received 12 March 2022; Received in revised form 12 September 2022; Accepted 18 September 2022
Available online 23 September 2022

Nomenclature

A_f	fibre cross-section area;
a_0	notch depth;
b	beam thickness;
c_0	concrete cover;
c_i	distance of the i-th reinforcing layer from the beam intrados;
E	matrix Young's modulus;
E_s	steel-bar Young's modulus;
$\{F\}$	bridging force vector;
F_i	bridging force of the i-th reinforcing layer;
h	beam depth;
K_I	global stress-intensity factor;
K_{IC}	concrete fracture toughness;
K_{Ii}	stress-intensity factor due to the i-th bridging force;
K_{IM}	stress-intensity factor due to the applied bending moment;
m	number of active reinforcing layers in the cross-section;
M	applied bending moment;
M_F	fracture moment;
$\widetilde{M}_F$	dimensionless fracture moment;
N_P	bar-reinforcement brittleness number;
$N_{P,f}$	fibre-reinforcement brittleness number;
N_{PC}	critical value of the bar-reinforcement brittleness number;
N_w	pull-out brittleness number;
n	total number of reinforcing layers in the cross-section;
n_b	steel-bar reinforcing layers in the cross-section;
n_f	fibre reinforcing layers in the cross-section;
V_f	fibre volume fraction;
$V_{f,min}$	minimum fibre volume fraction;
$\{w\}$	crack opening displacement vector;
w	crack opening displacement;
w_i	crack opening displacement at the i-th reinforcing layer;
w_c	critical crack opening displacement of the fibre reinforcement (fibre embedment length);
w_y	steel-bar yielding crack opening displacement;
$\{Y_F\}$	bridging force shape function vector;
Y_M	shape function related to the applied bending moment;
α	orientation factor;
γ_f	fibre specific weight;
Φ	steel-bar diameter;
φ	local rotation of the cross-section;
$\widetilde{\varphi}$	normalized local rotation;
λ_{MM}	local rotation compliance;
$[\lambda]$	matrix of the bridging force local compliances;
$\{\lambda_M\}$	vector of the bending moment local compliances;
ρ	steel-bar reinforcement percentage;
ρ_{min}	minimum steel-bar reinforcement percentage;
σ	bridging stress;
σ_i	bridging stress acting in the i-th reinforcing layer;
σ_s	fibre slippage strength;
$\overline{\sigma}_s$	generalized fibre slippage strength;
σ_y	steel-bar yielding stress;
τ_m	average shearing stress at the concrete-steel interface.

cohesive softening law —i.e., a stress vs crack opening relationship, σ-w— which includes both the toughening contributions of the concrete matrix and that of the reinforcing fibres. As suggested in Model Code 2010 [32], in the case of plain concrete, the contribution of the matrix can be modelled by a bi-linear softening curve, in which the describing parameters —i.e., the concrete fracture energy, G_F, and the concrete tensile strength, σ_t — are empirically correlated to the concrete compression strength or the concrete grade. On the other hand, in the case of FRC composites, a further contribution related to the toughening mechanism of the fibre is considered. In Fig. 1, the cohesive law of the composite is obtained as a superposition of the toughening contribution of concrete (thin dashed line)

and that of the reinforcing fibres (thin dot-dashed line). The area under the thick curve represents the fracture energy of the composite material, G_F.

Several experimental investigations evidenced how the presence of fibres leads to a variation in the shape of the composite constitutive law, which can be generally modelled by a multilinear function [33]. Moreover, the reinforcing fibres provide a significant increase in the critical crack opening displacement, w_{cr}, with a consequent increase (up to two orders of magnitude) in the fracture energy of the composite, G_F.

Generally speaking, due to the large number of variables involved in the FRC constitutive law, the latter is defined on the basis of experimental flexural tests. This design-by-testing procedure is required by the existing structural codes for the design of FRC members, where the post-cracking residual flexural strength at a given crack opening displacement is measured [32,34–35]. A similar approach can also be found in different research works, in which an inverse procedure is applied to identify the global σ-w constitutive relationship starting from a load–deflection or a load-CMOD experimental curve [36–38]. This single constitutive law could also be used in a sectional model that is able, on the basis of equilibrium, constitutive, and kinematic conditions, to predict the flexural response of FRC and HRC elements [10,13,16,19].

In all cases, the main drawback of the abovementioned approaches relies in the fact that the assumption of a single constitutive law for the fibrous composite —which is valid for a given percentage of reinforcing fibres, V_f— does not allow to capture the influence in the post-cracking regime of each single constituent of the composite. As a direct consequence, these approaches do not permit to predict directly the transition in the flexural response due to the change in fibre volume fraction, V_f.

In this work, the flexural behaviour of HRC members is captured in the framework of fracture mechanics by means of the Bridged Crack Model [39–48]. This model, which was originally proposed for the case of steel-bar reinforced concrete (RC) elements [39–41], has been recently applied to the case of FRC beams [49–53]. In the following, the simultaneous presence of steel-bars and reinforcing fibres is considered, leading to a further extension of the model to the case of HRC members. The assumption of the composite as a multi-phase material allows to capture the transitions affecting the post-cracking regime of the flexural response, which are found to be effectively described in terms of dimensionless numbers.

2. The Updated Bridged Crack Model (UBCM)

2.1. Fundamentals

In Fig. 2, the critical cross-section of a HRC beam subjected to bending is represented, where the following four regions can be identified: (i) ligament in compression; (ii) uncracked ligament in tension; (iii) reinforcement bridging zone, in which both short-fibres and steel-bars bridge the crack faces; (iv) stress-free crack zone, generally noticeable for large crack depths.

The Updated Bridged Crack Model (UBCM) focuses on the crack propagation phenomenon in a critical cross-section by assuming that the tensile cracking precedes other failure mechanisms, such as compression crushing and shear failure. In this respect, UBCM assumes the composite as a multi-phase material, in which the cementitious matrix and the reinforcing layers represent its primary and secondary phases, both contributing to the global toughening of the structural element.

Let us consider the rectangular cross-section of the HRC member to be characterized by a thickness, b, a depth, h, an initial notch depth, a_0, and to be subjected to an external bending moment, M (Fig. 2). Following the discontinuous formulation of the model [42–43], the total number of reinforcing layers in the cross-section, n, each one characterized by its own position c_i, is given by the sum of steel-bar reinforcement layers, n_b, and of the reinforcing fibres crossing the crack, n_f. The quantity n_b is known *a priori*, whereas n_f is strictly related to the fibre distribution within the volume of the composite. Following the suggestions given in [54], n_f can be calculated as:

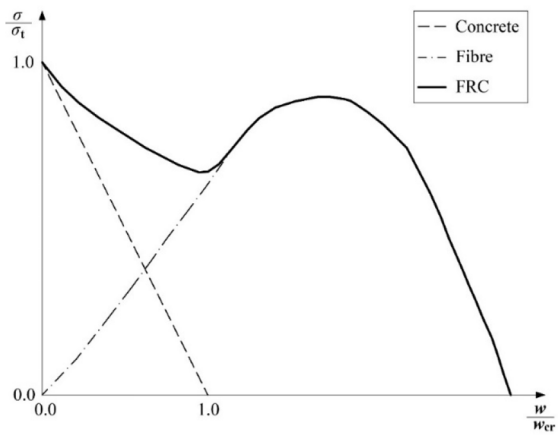

Fig. 1. Cohesive law of FRC composite as a mono-phase material: Superposition of matrix and fibre-reinforcement contributions.

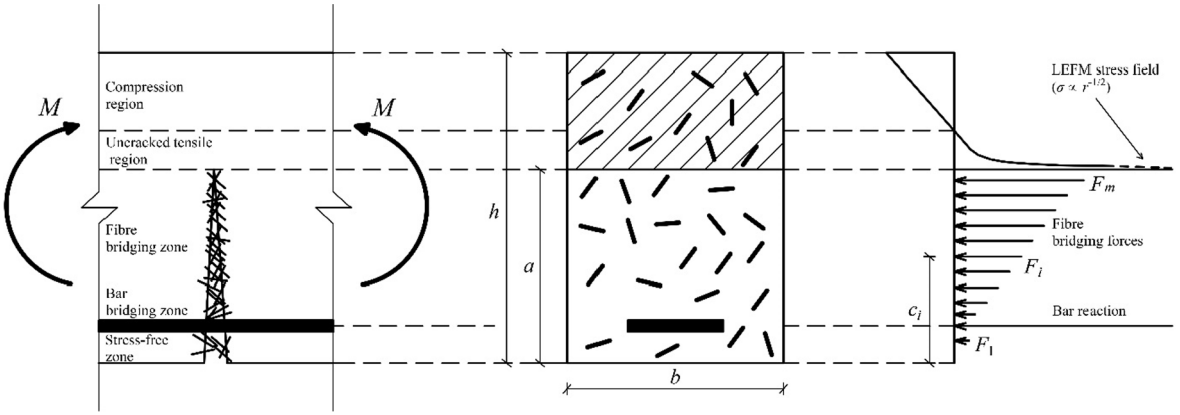

Fig. 2. Critical cross-section in HRC beam and stress distribution predicted by the UBCM.

$$n_f = \alpha V_f \frac{bh}{A_f}, \tag{1}$$

where A_f is the cross-sectional area of the single fibre, and α the orientation factor. The latter, which is defined as the ratio between the actual number of fibres in the critical cross-section and the theoretical one, can be experimentally found by investigating the specimen fracture surface at the end of the experimental tests, or predicted on the basis of statistical tools able to model the fibre distribution within the volume of the specimen.

Among the total number of reinforcing layers, some of them, m, are considered as active since they bridge the crack faces during the crack propagation process. Their toughening contribution is described by a distribution of bridging forces (see the right part of Fig. 2), F_i, which depends on the reinforcement constitutive laws. The latter describe the yielding of the steel-bars and the pull-out of the short-fibres. In terms of closing stresses, they can be written as:

$$\text{for } i = 1, \cdots, m \quad \sigma_i = f(w_i), \tag{2}$$

providing a set of m equations which relate the stress acting in the i-th active reinforcement, σ_i, with the corresponding crack opening displacement, w_i. These constitutive laws will be discussed in the following.

By assuming the concrete matrix as a linear-elastic perfectly-brittle material —other nonlinear contributions (in tensile and compression behaviours) are considered as negligible— a $r^{-1/2}$ stress singularity is predicted at the crack tip (Fig. 2), which is characterized by a global stress-intensity factor, K_I:

$$K_I = K_{IM} - \sum_{i=1}^{m} K_{Ii} = \frac{M}{bh^{3/2}} Y_M - \frac{\{Y_F\}^T \{F\}}{bh^{1/2}}. \tag{3}$$

The contributions related to the applied bending moment, K_{IM}, and to the i-th reinforcing layer, K_{Ii}, appear in Eq. (3). The crack propagation occurs when the stress-intensity factor, K_I, reaches its critical value, K_{IC}, i.e., the fracture toughness of the plain matrix (unreinforced material) [55].

Finally, a set of compatibility conditions is needed to calculate the crack opening, w_i, at each i-th active reinforcement level as a function of the applied bending moment, M, and of the bridging forces, F_i. In matrix form, we have:

$$\{w\} = \{\lambda_M\} M - [\lambda]\{F\}, \tag{4}$$

where $\{w\}$ is the crack opening vector, $\{\lambda_M\}$ is the vector of the local compliances due to the bending moment, and $[\lambda]$ is the matrix of the local compliances due to the bridging forces. The local compliances, i.e., the influence coefficients $\lambda_{M,i}$ and λ_{ij}, are obtained by considering the strain energy release rate of a cracked element subjected to a bending moment and to a distribution of closing forces applied on the crack faces. The calculation procedure is extensively explained in [42].

For a given crack depth, the problem relies in the determination of the $2m + 1$ unknowns, i.e., the fracture moment, M_F, the profile of the crack opening displacements, $\{w\}$, and the corresponding distribution of bridging forces, $\{F\}$, related to both active steel-bars and reinforcing fibres. The analytical solution is obtained by means of an iterative procedure, which is based on the reinforcement constitutive laws (Eq. (2)), on the equilibrium (crack propagation) condition (Eq. (3)), and on the displacement compatibility conditions (Eq. (4)).

More precisely, for a given crack depth, the procedure is based on the following steps:

(i) Determination of the number of active reinforcing layers, m;
(ii) Calculation of the local compliances;
(iii) Assumption of a trial crack opening profile;

(iv) Determination of the corresponding set of bridging forces (Eq. (2));
(v) Calculation of the fracture moment (Eq. (3));
(vi) Calculation of the crack opening displacements (Eq. (4));
(vii) Checking the convergence between step (vi) and step (iii).

Following this routine, it is possible to evaluate the stress-profile (Fig. 2) for each crack depth. Then, by repeating the above-mentioned procedure, it is possible to thoroughly describe the fracturing process up to the complete disconnection of the HRC cross-section. This routine, which was implemented in Matlab environment, has been used to obtain the parametric analyses and the numerical vs experimental comparisons that will be shown later in the paper.

2.2. Reinforcement constitutive laws

In the framework of fracture mechanics, the reinforcement constitutive laws are defined in terms of stress vs crack opening displacement relationships.

In the case of steel-bars, their toughening action can be described by an hardening-perfectly plastic constitutive law, which is schematically represented in Fig. 3a, and it is analytically defined as follows:

$$\text{for } 0 < w < w_y: \qquad \sigma(w) = \sigma_y \left(\frac{w}{w_y}\right)^{\lambda}, \tag{5a}$$

$$\text{for } w \geq w_y: \qquad \sigma(w) = \sigma_y, \tag{5b}$$

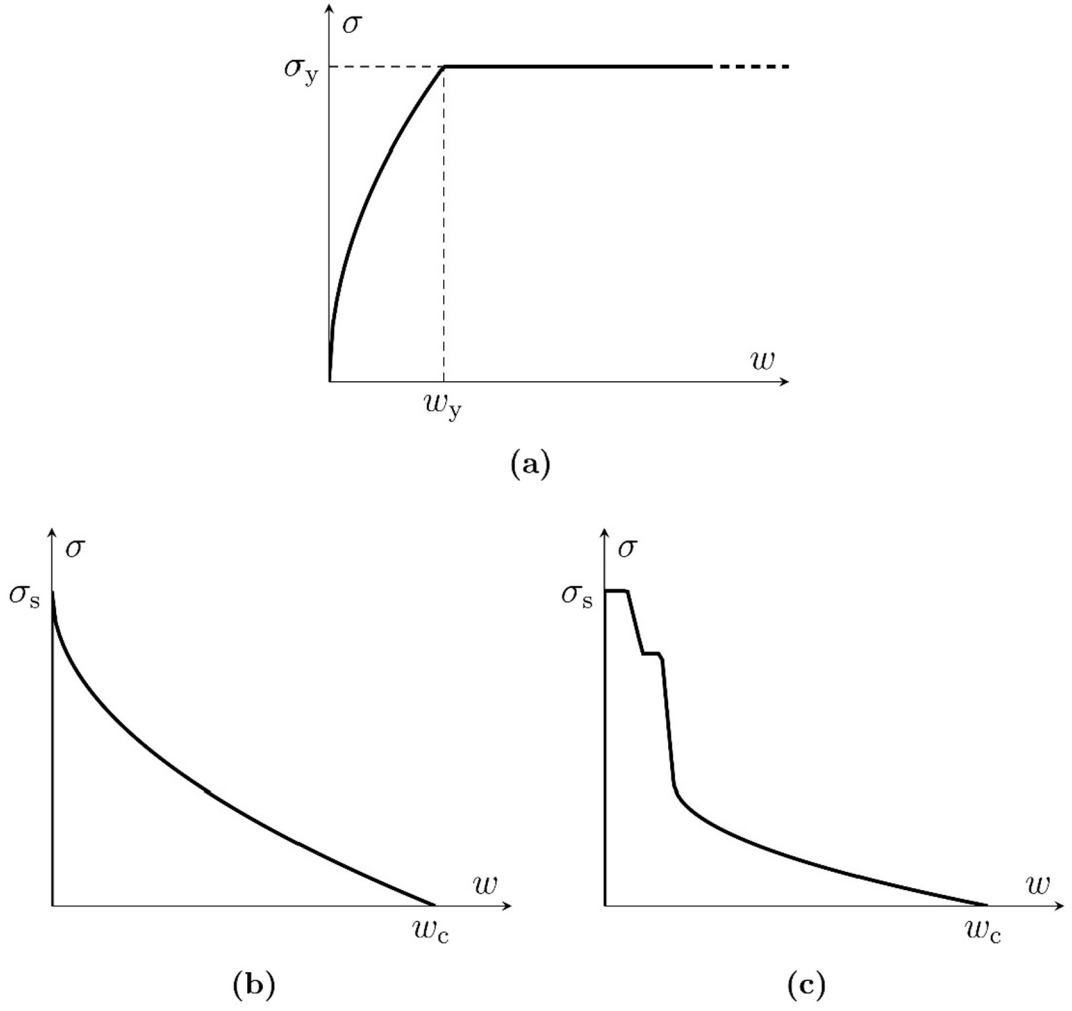

Fig. 3. Reinforcement constitutive laws: (a) Hardening-perfectly plastic constitutive law of the steel-bar; (b) Rigid-softening constitutive law of the straight steel-fibre; (c) Rigid-softening constitutive law of the hooked-end steel-fibre.

where σ_y is the yield strength, w_y is the corresponding crack opening displacement, and λ is the power-law exponent which governs the initial branch of the constitutive law prior to steel-bar yielding. Following the bond-slip model previously proposed by Ruiz et. al [56], λ is assumed to be equal to 1/2, whereas w_y can be estimated as a function of σ_y, of the steel-bar diameter, Φ, of the steel Young's modulus, E_s, and of the average shearing stress at the concrete-steel interface, τ_m:

$$w_y = \frac{\sigma_y^2 \Phi}{4 E_s \tau_m}. \tag{6}$$

It is worth noting that the assumed constitutive law does not consider the hardening behaviour that occurs after the steel-bar yielding, as well as the possible rupture of the rebar.

On the other hand, the constitutive law adopted for the fibres describes the pull-out of the short reinforcements from the cementitious matrix. The slippage mechanism of the fibres is typically investigated by means of pull-out tests carried out on a single fibre. Extensive experimental campaigns evidenced that the pull-out behaviour of the fibres is significantly affected by different factors, among which we have: the fibre material (steel, polymer, etc.), the fibre geometry (straight, crimped, twisted, with hooked ends, etc.), the mechanical properties of the matrix, the orientation of the fibre with respect to the direction of the pull-out load [57–59].

An interesting attempt to define a unified constitutive law for fibre-reinforcements was made by Abdallah et al. [60], who have recently proposed a generalized pull-out law per unit embedded length of the fibre, in the case of straight or hooked-end steel fibres. The two constitutive laws are represented in Fig. 3 (b)-(c), where the stress in the fibre, σ, is plotted as a function of the relative slip (or crack opening displacement), w, in terms of normalized coordinates. The laws take into account the slippage strength of the fibre, σ_s, beyond which the fibre pull-out is triggered, and the embedded length of the fibre, w_c, representing the slip (or crack opening) beyond which the fibre is entirely pulled-out from the matrix, then exhausting its bridging effect. Thus, the authors define a shape of the constitutive law that does not change by varying σ_s and/or w_c. It is worth noting that the pull-out strength of the fibre is described by the axial stress σ_s, which is a function of the maximum pull-out force due to the distribution of the shear stresses, τ, acting along the embedded length at the fibre–matrix interface.

In the case of straight steel fibres, function $\sigma(w)$ can be analytically defined as follows:

$$w = 0, \qquad \text{if } \sigma(w) < \sigma_s, \tag{7a}$$

$$\text{for } w \geq 0: \qquad \sigma(w) = \sigma_s \left(1 - \left(\frac{w}{w_c}\right)^{0.5}\right). \tag{7b}$$

On the other hand, in the case of hooked-end steel fibres:

$$w = 0, \qquad \text{if } \sigma(w) < \sigma_s, \tag{8a}$$

$$\text{for } 0 < w < 0.06\, w_c: \qquad \sigma(w) = \sigma_s, \tag{8b}$$

$$\text{for } 0.06\, w_c < w < 0.10\, w_c: \sigma(w) = \sigma_s \left(1 - 0.2\left(\frac{w - 0.06 w_c}{0.10 w_c - 0.06 w_c}\right)\right), \tag{8c}$$

$$\text{for } 0.10\, w_c < w < 0.15\, w_c: \qquad \sigma(w) = 0.8\sigma_s, \tag{8d}$$

$$\text{for } 0.15\, w_c < w < 0.18\, w_c: \quad \sigma(w) = \sigma_s \left(0.8 - 0.4\left(\frac{w - 0.15 w_c}{0.18 w_c - 0.15 w_c}\right)\right), \tag{8e}$$

$$\text{for } 0.18\, w_c < w < w_c: \quad \sigma(w) = 0.4\sigma_s \left(1 - \left(\frac{w - 0.18 w_c}{w_c - 0.18 w_c}\right)^{0.5}\right), \tag{8f}$$

$$\text{for } w \geq w_c: \qquad \sigma(w) = 0. \tag{8g}$$

Eqs. (7a), (7b), (8a)–(8f) do not consider the tensile failure of the fibre, which can occur for high orientation angles of the fibre with respect to the applied load [59], or when high-strength matrices are used in combination with normal-strength fibres [23–26].

2.3. HRC cross-sectional response and dimensionless numbers

For a given crack depth, the local rotation of the HRC cross-section can be calculated as follows:

$$\varphi = \lambda_{MM} M - \{\lambda_M\} \mathrm{T} \{F\}. \tag{9}$$

The involved local compliances, λ_{MM} and λ_{Mi}, are calculated by following the procedure already mentioned in the case of the coefficients appearing in Eq. (4). The global deflection, δ, of the beam can be calculated by applying the superposition principle, according to which the total deflection takes into account both the nonlinear contribution related to the cracking process occurring at the critical section (inelastic hinge), and that related to the elastic behaviour of the remaining part of the specimen. In Fig. 4, the

application of the principle is schematically shown in the case of a three-point bending test.

Under these assumptions, the UBCM predicts different post-cracking regimes as a function of three scaling dimensionless numbers, i.e., the *bar-reinforcement brittleness number*, N_P, the *fibre-reinforcement brittleness number*, $N_{P,f}$, and the *pull-out brittleness number*, N_w, which are defined as follows:

$$N_P = \rho \frac{\sigma_y}{K_{IC}} h^{1/2}, \tag{10}$$

$$N_{P,f} = V_f \frac{\alpha \sigma_s}{K_{IC}} h^{1/2} = V_f \frac{\overline{\sigma}_s}{K_{IC}} h^{1/2}, \tag{11}$$

$$N_w = \frac{E w_c}{K_{IC} h^{1/2}}. \tag{12}$$

The bar-reinforcement brittleness number, N_P (Eq. (10)), depends on the steel-bar reinforcement percentage, ρ, on the steel yield strength, σ_y, on the matrix fracture toughness, K_{IC}, as well as on the beam depth, h. An analogous expression (Eq. (11)) can be obtained for the fibre-reinforcement brittleness number, $N_{P,f}$, by replacing the bar-reinforcement parameters, ρ and σ_y, with the fibre volume fraction, V_f, and the generalized slippage strength of the fibre, $\overline{\sigma}_s$, respectively. It should be noted that $\overline{\sigma}_s$ englobes the orientation factor, α. Finally, the pull-out brittleness number, N_w (Eq. (12)), depends on the equivalent embedded length of the fibre, w_c, on the matrix Young's modulus, E, on the matrix fracture toughness, K_{IC}, and on the beam depth, h. The abovementioned dimensionless numbers, N_P, $N_{P,f}$, and N_w, are affected by the structural size, h, an increase in h providing an increase in N_P and $N_{P,f}$, and a decrease in N_w.

3. Numerical simulations

In this section, several sets of numerical analyses are presented in order to highlight the influence of the three dimensionless numbers, N_P, $N_{P,f}$, and N_w, on the structural response of lightly RC, FRC, and HRC beams. In all cases, the flexural response is described in terms of dimensionless fracture moment, $\widetilde{M}_F = \frac{M_F}{K_{IC} b h^{3/2}}$, vs local normalized rotation, $\widetilde{\varphi} = \varphi \frac{E h^{1/2}}{K_{IC}}$, diagrams.

A rectangular cross-section, characterized by thickness and depth of 150 mm, and an initial notch of depth equal to 0.15 h, has been considered in the numerical analyses. The cementitious matrix is characterized by a fracture toughness of 30 MPa mm$^{1/2}$ and a Young's modulus of 30 GPa. The steel-bar reinforcement phase has been modelled by a single reinforcing layer and by a concrete cover equal to the initial notch depth ($a_0/h = c_0/h = 0.15$). A yielding strength of 500 MPa and the corresponding crack opening displacement equal to 0.40 mm define the constitutive law of the continuous reinforcement. The toughening action of the short-fibres is represented by a distribution of reinforcing layers, which are evenly spaced within the ligament area. A slippage strength of 200 MPa has been considered. By keeping unchanged the parameters listed above, and by varying the steel-bar percentage, ρ, the fibre volume fraction, V_f, and the fibre embedment length, w_c, it is possible to govern the corresponding variation in the three brittleness numbers on the basis of Eqs. (10)–(12).

In Fig. 5, the numerical curves refer to the case of lightly RC beam ($\rho \neq 0$; $V_f = 0$). They are traced by varying the steel-bar area percentage, ρ, up to 0.25 %, thus providing the corresponding variation in the *bar-reinforcement brittleness number*, N_P, from 0 to 0.50 (Eq. (10)). The latter governs the ductile-to-brittle transition in the post-cracking regime of the response, leading to define the critical condition —ultimate bending moment (circle markers) equal to the first cracking moment (square marker) of the section— for which a stable post-peak response is guaranteed. At the critical condition, the corresponding value of the brittleness number, N_{PC}, depending on

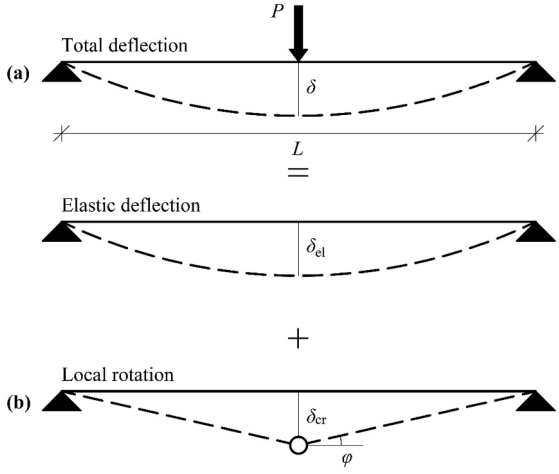

Fig. 4. Superposition principle of elastic deflection and local rotation of the beam.

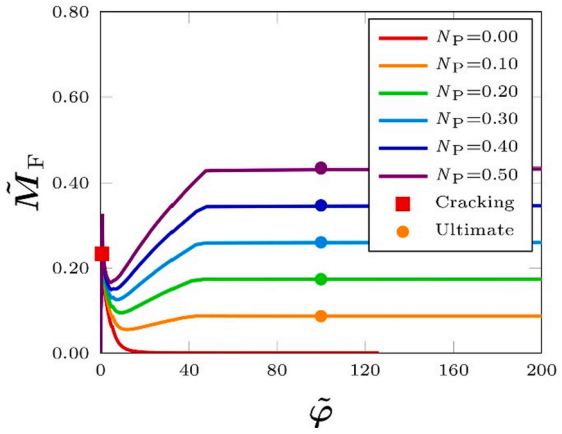

Fig. 5. Dimensionless fracture moment vs local rotation of lightly RC beams by varying N_P.

a_0/h and c_0/h, permits to calculate the minimum steel-bar reinforcement percentage, ρ_{min}. In the case under investigation, N_{PC} ($a_0/h = c_0/h = 0.15$) is found to be equal to 0.28.

On the other hand, when the UBCM is applied to the case of FRC ($\rho = 0$; $V_f \neq 0$), two dimensionless numbers are required to fully describe the post-cracking behaviour of the composite.

As discussed in previous papers [50–53], the fibre-reinforcement brittleness number, $N_{P,f}$, plays the analogous role of N_P for lightly RC beams, since it affects the FRC load-bearing capacity and defines the minimum reinforcement condition of the composite structure. Moreover, the pull-out brittleness number, N_w, takes into account the effect of the reinforcing fibre length, thus governing the decrease in the fibre toughening contribution due to its progressive slippage.

In Fig. 6a, the moment vs rotation curves are plotted by varying V_f from 0 to 1.25 %, for a given value of w_c equal to 25 mm. Considering Eqs. (11)–(12), $N_{P,f}$ ranges from 0 to 1.00, whereas N_w is constant and equal to 2041. It clearly emerges how, unlike the previous case (Fig. 5), the influence of $N_{P,f}$ is restricted to the intermediate stage (Stage II) of the flexural response, in which the load bearing capacity (circle markers) is defined. This is due to N_w, which drives the decrement in the applied moment in the final stage (Stage III) of the response, providing the convergence of all the curves to a single softening tail. In the case under investigation ($a_0/h = 0.15$), the critical value of $N_{P,f}$ is equal to 0.56

Analogous conclusions can be drawn for Fig. 6b, where the flexural response of the FRC beam is plotted by varying w_c from 0 to 25 mm, for a given value of $N_{P,f}$ equal to 1.00 ($V_f = 1.25$ %). In this case, the post-cracking behaviour is characterized by the same intermediate stage until the curves slip towards different softening branches depending on the value of N_w.

The structural behaviour of HRC ($\rho \neq 0$; $V_f \neq 0$) can be represented as a combination of the two previous cases, in which, due to the simultaneous presence of both steel-bars and short-fibres, all the three brittleness numbers affect the global flexural response.

In Fig. 7a, a family of curves is obtained by varying N_P, whereas the brittleness numbers related to the fibre-reinforcement, $N_{P,f}$ and N_w, are kept unchanged ($N_{P,f} = 0.20$; $N_w = 1225$). It is evident how N_P affects the whole post-cracking regime, thus providing a significant contribution in terms of global toughening and structural ductility/stability. In strong analogy to the case of FRC, the

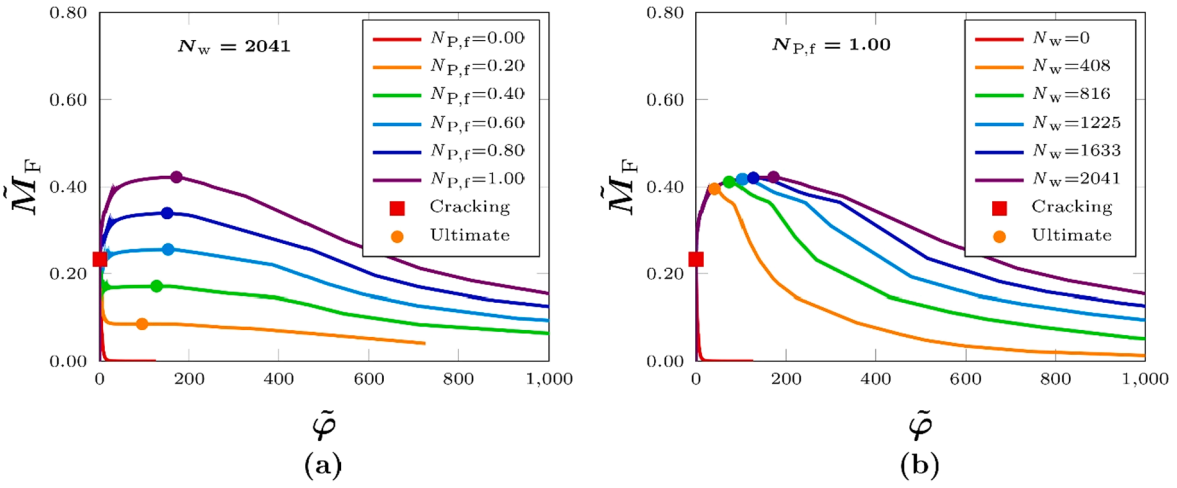

Fig. 6. Dimensionless fracture moment vs local rotation of FRC beams: **(a)** Influence of $N_{P,f}$; **(b)** Influence of N_w.

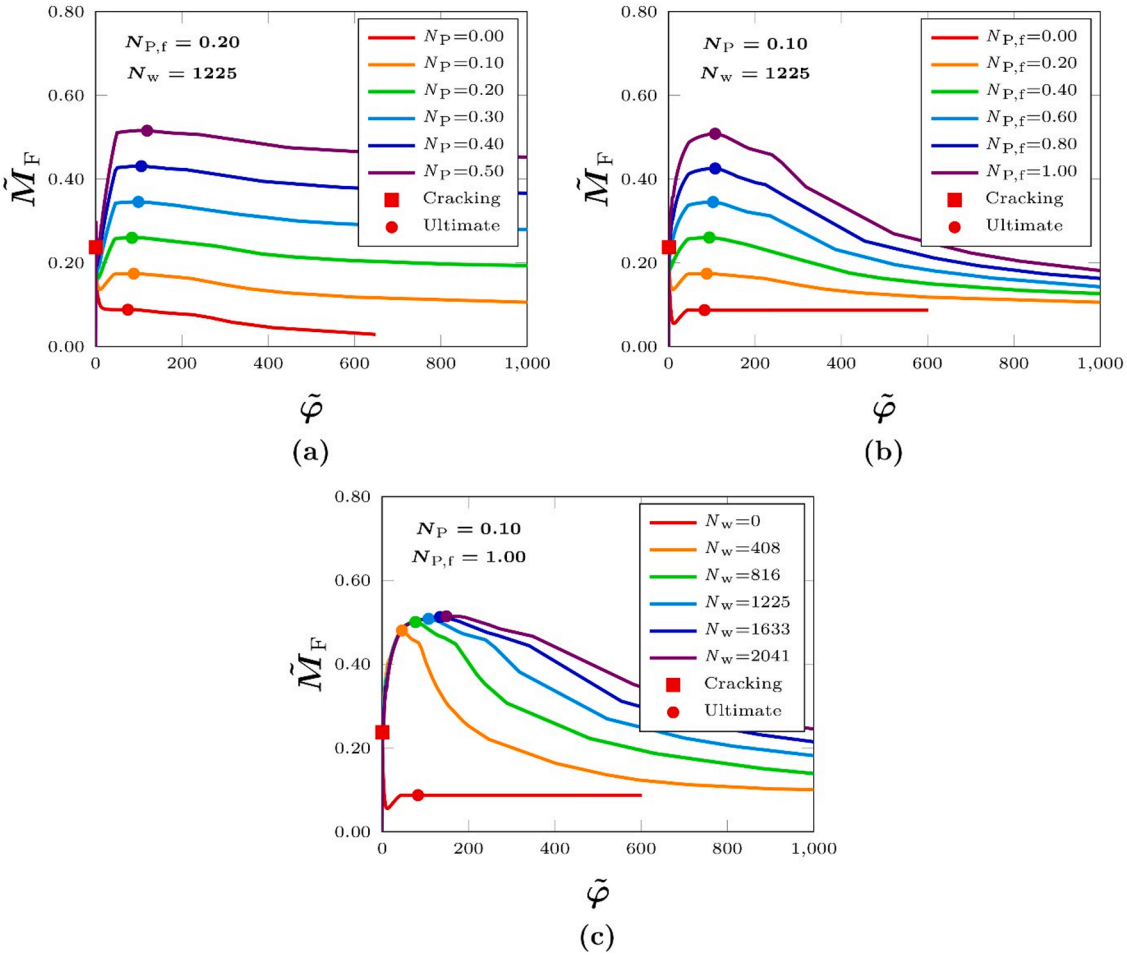

Fig. 7. Dimensionless fracture moment vs local rotation of HRC beams: **(a)** Influence of N_P; **(b)** Influence of $N_{P,f}$; **(c)** Influence of N_w.

numerical curves suggest to identify-three stages being characterized by the flexural response of the HRC beam. In Stage I, the specimen exhibits a linear elastic behaviour. At the onset of the fracturing process (red square marker), the post-cracking regime takes place, being characterized by an intermediate stage (Stage II), in which both steel-bars and fibres contribute to the load bearing capacity (circle markers). In the final stage (Stage III), which describes the gradual exhaustion of the fibre toughening contribution, the curves tend towards different plastic plateaus, each one defined by its corresponding steel-bar reinforcement brittleness number, N_P. It is worth noting that the case of $N_P = 0$ (see the red curve in Fig. 7a) reproduces the case of FRC (see the orange curve in Fig. 6a) where the final plastic plateau coincides with the abscissae axis.

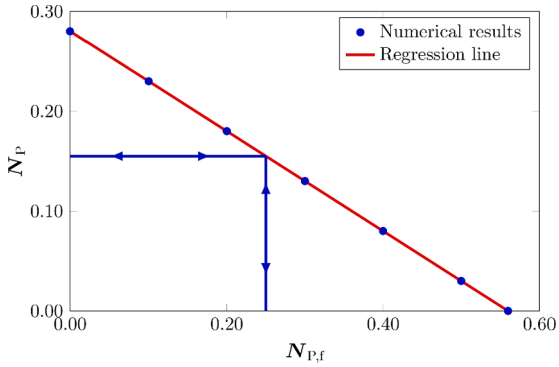

Fig. 8. Minimum reinforcement design nomograph for HRC beams.

In addition, a variation in the fibre-reinforcement brittleness number, $N_{P,f}$ (Fig. 7b) affects just Stage II of the flexural response. Consistently with previous discussions, Stage III is characterized by an asymptotic convergence of all the curves to a common plastic plateau, which is defined by N_P. Moreover, even if the amount of steel-bar reinforcement, i.e., N_P, is not sufficient to provide a stable post-peak response ($N_P < N_{PC} = 0.28$), the additional contribution represented by the reinforcing fibres, i.e., $N_{P,f}$, permits to obtain an ultimate bending moment greater than the first cracking moment (see the green, cyan, blue, and purple curves in Fig. 7b). In this sense, the crucial point is that the minimum reinforcement condition in HRC beams can be obtained by an effective combination of N_P and $N_{P,f}$.

Finally, the set of curves in Fig. 7c is obtained by varying N_w and keeping unchanged the reinforcement brittleness numbers, N_P and $N_{P,f}$ ($N_P = 0.10$; $N_{P,f} = 1.00$). Even if N_w affects the exhaustion of the fibre toughening effect, there is no significant influence on the load bearing capacity of the HRC specimen (circle markers), as well as on the final plastic plateau shown in the structural response.

In order to evaluate the minimum reinforcement conditions in HRC beams, in Fig. 8 each point corresponds to a combination of the two reinforcement brittleness numbers, N_P and $N_{P,f}$, required to obtain a stable post-peak response of the composite beam (ultimate bending moment equal to the first cracking moment). It is found that, in the critical conditions, N_P and $N_{P,f}$ can be effectively interpolated by a linear relation, defining in this way the minimum reinforcement design of HRC beams. The minimum reinforcement curve divides the nomograph into two regions, corresponding to a safe (upper part) or unsafe (lower part) behaviour of the HRC beam. For a given value of N_P —i.e., a certain percentage of steel-bar reinforcement, ρ—, it is possible to obtain the corresponding value of $N_{P,f}$ —i.e., the fibre volume fraction, V_f— required to obtain the minimum reinforcement condition, and *vice-versa*. In brief, the nomograph of Fig. 8 can be proposed as an effective tool for a quantitative evaluation of the amount of reinforcing fibres necessary to a partial (or total) replacement of steel-bars in HRC structures in flexure.

4. Experimental validation

In the following, an extensive experimental campaign recently carried out by Holschemacher et al. [17] is taken into consideration. The effects of different types of steel-fibres on the mechanical properties of reinforced high-strength concrete beams are investigated. In addition to compression and splitting tests, four-point bending tests were performed to investigate the flexural behaviour of high-strength concrete beams reinforced with steel-bars and steel-fibres. The test geometry is schematically represented in Fig. 9, where the prismatic specimen is characterized by a length of 700 mm, a span of 600 mm, a thickness of 150 mm, and a depth of 150 mm.

The concrete mixture is characterized by a 28-day average cubic compression strength of 86 MPa. Three different fibre types are considered. Two hooked-end steel-fibre types, F1 and F2, are characterized by the same geometry but different nominal tensile strengths, equal to 1100 and 1900 MPa, respectively. In addition, one corrugated steel-fibre type, F3, is tested. Further information about the properties of the abovementioned fibres can be found in [17]. For each fibre type, four different fibre volume fractions were considered: 0, 20, 40, and 60 kg/m^3. On the other hand, three different steel-bar reinforcement percentages were adopted: 0, 0.25 % (2Φ6), and 1.00 % (2Φ12). The nominal yield strength of the steel-bars was reported to be equal to 500 MPa. For each specimen series —corresponding to a certain combination of fibre-type, fibre volume fraction, and steel-bar reinforcement ratio— six flexural tests were performed in order to average the experimental results.

As discussed in Section 2.1, UBCM can be applied to reinforced members where the cracking failure precedes other possible failure modes, e.g., concrete compression crushing and shear failure. Considering the experimental campaign under investigation [17], it is reported that the specimens with higher reinforcement percentage ($\rho = 1.00$ %) experienced concrete crushing, shear failure, or a combination of these two collapse mechanisms (see Table 4 in [17]). As a consequence, these specimens are excluded from the present investigation, thus restricting the applicability of the model to the specimens characterized by lower steel-bar reinforcement percentages (0 and 0.25 %), which experienced cracking failure as main collapse mechanism. In addition, the specimens reinforced with corrugated fibres are not taken into consideration in the following analyses.

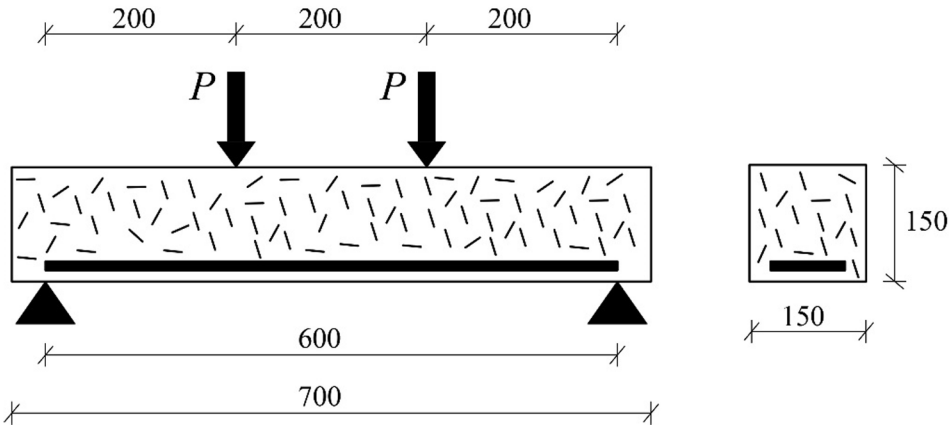

Fig. 9. Test geometry [17].

4.1. Identification of the mechanical properties

The application of the UBCM requires the constitutive parameters of the matrix (concrete fracture toughness, K_{IC}), of the steel-bar (yield strength, σ_y), and of the steel-fibres (slippage strength, $\overline{\sigma}_s$, and the fibre embedment length, w_c).

The concrete fracture toughness, K_{IC}, can be determined by performing fracture tests on notched specimens of plain concrete. In the case under consideration, K_{IC} has been identified by considering the peak load measured during the flexural tests (4PBT) carried out on nominally unnotched specimens of plain concrete (A-0 in [17]). By assuming a fictitious notch of depth $a_0 = 0.15\ h$ to model the concrete cover, a fracture toughness equal to 64 MPa mm$^{1/2}$ has been obtained (Table 1). The superposition between the experimental curve and the numerical prediction is represented in Fig. 10a.

On the other hand, the steel-bar yield strength, σ_y, is typically determined by means of tensile tests carried out on single rebars. In this respect, in [17] it is found σ_y equal to 500 MPa, according to German standards. Nevertheless, by considering the plastic plateau experienced by the RC specimen B-0, it is clear how the declared value represents a lower bound for the actual yield strength. In fact, by imposing the equilibrium at the complete disconnection of the cross-section, it results that σ_y is very close to 800 MPa. This consideration is confirmed by the numerical prediction provided by UBCM, which is in strong agreement with the corresponding experimental result (see Fig. 10b).

Finally, the model requires the identification of the constitutive parameters related to the short-fibres, $\overline{\sigma}_s$ and w_c. Analogously to the case of the continuous rebars, this information could be obtained by means of pull-out tests carried out on the single reinforcing fibre. Following this route, the obtained results would refer to a single fibre without considering the actual distribution of the short reinforcements within the volume of the composite, i.e., in the critical cross-section. As a consequence, when dealing with FRC, it seems more reasonable to identify the values of $\overline{\sigma}_s$ and w_c on the basis of the flexural tests on FRC specimens. For the experimental campaign under investigation, an identification procedure, already used by the authors in recent works [51–53], has been applied to FRC specimens A-20, A-40, and A-60 [17], as shown in Fig. 10c and Table 1.

4.2. Prediction of HRC flexural response

Considering the identification procedure previously discussed, the prediction of the HRC flexural response is carried out by considering the concrete fracture toughness, K_{IC}, equal to 64 MPa mm$^{1/2}$, the yielding strength, σ_y, equal to 800 MPa, the fibre slippage strength, $\overline{\sigma}_s$, equal to 462 MPa, and the fibre embedment length, w_c, equal to 10 mm. The yielding crack opening displacement, w_y, is calculated by means of Eq. (6) considering the mechanical properties declared in [17], and it is found to be equal to 0.60 mm.

When the mechanical properties of each phase of the composite are identified, the flexural response of FRC and HRC specimens can be predicted as a function of the fibre volume fraction, V_f, and of the steel-bar reinforcement percentage, ρ. The superposition between experimental data (dotted curves) and numerical predictions (continuous curves) is represented in Fig. 11 for the specimens under investigation. In all cases, a good agreement between numerical and experimental curves is obtained.

The influence of the reinforcing phases, i.e., the steel-bars and the steel-fibres, on the flexural response is clearly captured by the model. The fibres avoid the unstable crack propagation in FRC specimens (Fig. 11a) and provide an additional contribution in terms of load bearing capacity of HRC specimens (Fig. 11b). In the latter case, the contribution of the steel-bar reinforcing phase makes the flexural response as characterized by a final plastic plateau different from zero.

In the framework of the UBCM, these different behaviours can be synthetically described in terms of brittleness numbers, which are reported in Table 2. It can be noted that, for given values of the mechanical properties, the variation in ρ and V_f affects N_P and $N_{P,f}$ according to Eqs. (10) and (11), respectively. N_P varies from 0 to 0.38, whereas $N_{P,f}$ varies from 0 to 0.66. On the other hand, the pull-out brittleness number, N_w, remains unchanged ($N_w = 531$).

Considering the stability of the post-cracking response, the minimum reinforcement condition is achieved in one case among the FRC specimen series (curve A-60), being the first cracking moment almost equal to the load-bearing capacity. Moreover, in the case of HRC specimens (Fig. 11b), a stable post-cracking response is experimentally observed in all cases. It is worth noting that, in these cases, the amount of steel-bar area is sufficient to guarantee the minimum reinforcement condition regardless of the addition of steel-fibres.

Table 1
Identified mechanical properties.

ID	Fibre-type	ρ (%)	$V_f\ \gamma_f$ (kg/m^3)	K_{IC} (MPa mm$^{1/2}$)	$\overline{\sigma}_s$(MPa)	w_c (mm)	σ_y(MPa)
A-0 (plain concrete)	–	0	0	64	–	–	–
B-0 (RC)	–	0.25	0	–	–	–	800
A-20 (FRC)	F1	0	20	–	524	12.5	–
A-40 (FRC)	F1	0	40	–	454	9	–
A-60 (FRC)	F1	0	60	–	408	9.5	–
Avg.	–	–	–	64	462	10	800

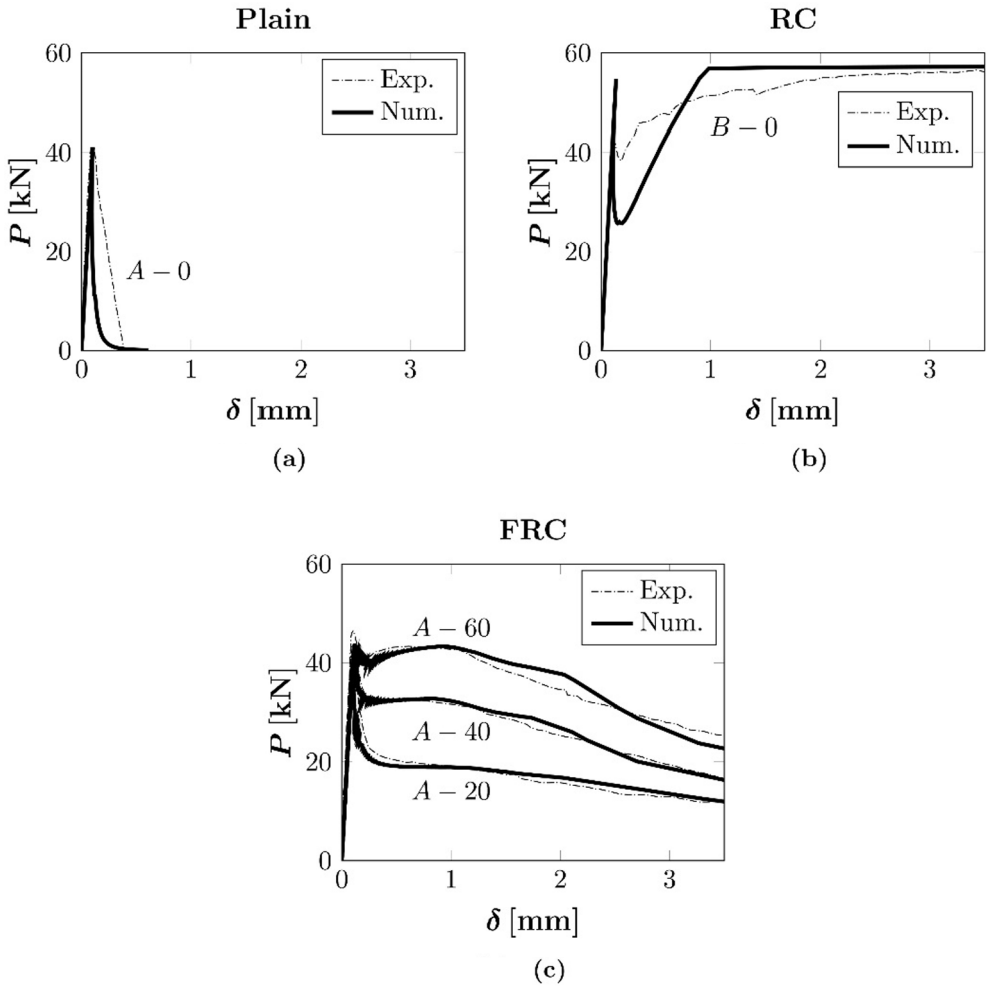

Fig. 10. Identification of the experimental curves: **(a)** Plain concrete; **(b)** Reinforced concrete (RC); **(c)** Fibre-reinforced concrete (FRC).

In fact, in all cases the bar-reinforcement brittleness number, N_P, is found to be greater than its critical value (0.28).

In this context, it is possible to predict the minimum reinforcement condition of the HRC beams, which is defined as the effective combination of ρ_{min} and $V_{f,min}$ able to guarantee a stable post-peak response. By using the nomograph of Fig. 8, it can be observed that different combinations of N_P and $N_{P,f}$ allow to obtain a stable structural response.

The two limit conditions are indicated with a thick line in Fig. 12, together with the experimental curves (dashed thin lines) previously analysed. The corresponding brittleness numbers, in the case of FRC and RC specimens, are respectively: (i) $N_{P,f} = 0.56$ and $N_P = 0$; (ii) $N_{P,f} = 0$ and $N_P = 0.28$. Considering the identified mechanical properties of the composite (Table 2), the two limit conditions correspond to: (i) $V_{f,min}$ equal to 0.63 %; (ii) ρ_{min} equal to 0.19 %. These two curves identify a region in which all the possible minimum reinforcement combinations predicted by UBCM are included.

5. Conclusions

The minimum reinforcement condition in hybrid-reinforced concrete beams is interpreted in the framework of fracture mechanics by means of the Updated Bridged Crack Model (UBCM). The model assumes the reinforced element as a multi-phase composite, in which the cementitious matrix (primary phase) is assumed to be linear-elastic perfectly-brittle. On the other hand, different nonlinear constitutive laws are used to model the behaviour of the reinforcing phases, considering the yielding of the steel-bar reinforcements and the slippage of the short fibres.

The ductile-to-brittle transitions characterizing the structural behaviour are governed by three scaling dimensionless numbers: the bar-reinforcement brittleness number, N_P, which describes the toughening contribution of the steel-bar reinforcement; the fibre-reinforcement brittleness number, $N_{P,f}$, and the pull-out brittleness number, N_w, which both describe the toughening contribution of the reinforcing fibres. The minimum reinforcement condition in hybrid-reinforced concrete structures is proved to be obtained by an effective combination of N_P and $N_{P,f}$.

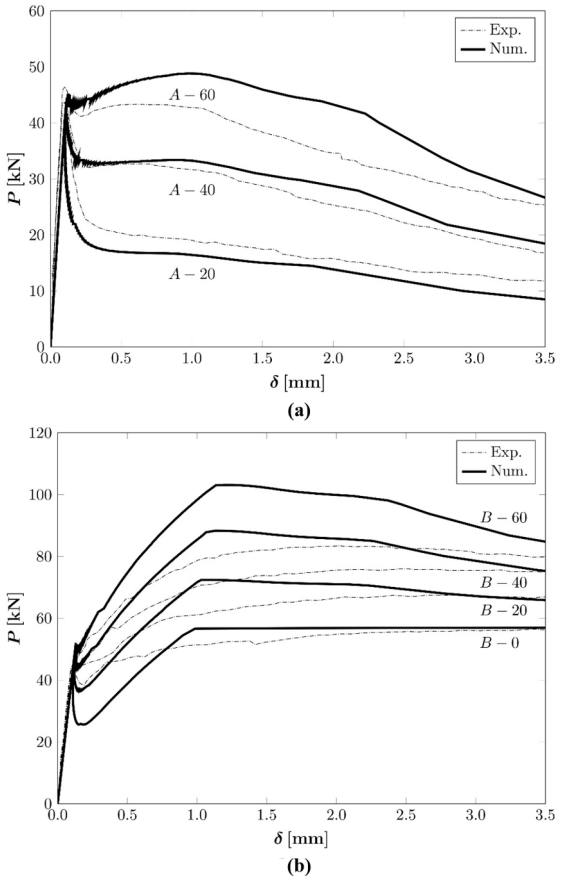

Fig. 11. Prediction of the experimental curves: **(a)** FRC; **(b)** HRC.

Table 2
Brittleness numbers.

ID	Fibre-type	ρ (%)	$V_f \gamma_f$ (kg/m^3)	K_{IC} (MPa mm$^{1/2}$)	$\bar{\sigma}_s$(MPa)	w_c (mm)	σ_y(MPa)	N_P (-)	$N_{P,f}$ (-)	N_w (-)
A-20	F1	0	20	64	462	10	–	0	0.22	531
A-40	F1	0	40	64	462	10	–	0	0.45	531
A-60	F1	0	60	64	462	10	–	0	0.66	531
B-0	–	0.25	0	64	–	–	800	0.38	0	–
B-20	F1	0.25	20	64	462	10	800	0.38	0.22	531
B-40	F1	0.25	40	64	462	10	800	0.38	0.45	531
B-60	F1	0.25	0	64	462	10	800	0.38	0.66	531

The effectiveness of the model is discussed on the basis of a recent experimental campaign, in which the structural behaviour of hybrid-reinforced concrete beams is investigated. The substantial overlapping between numerical predictions and experimental results suggests the full applicability of the model as a design-by-testing procedure to determine the minimum reinforcement conditions for hybrid-reinforced concrete beams, thus promoting the fibres as an effective partial or total replacement of traditional steel-bars.

CRediT authorship contribution statement

Federico Accornero: Writing – original draft, Methodology, Formal analysis, Conceptualization. **Alessio Rubino:** Software, Data curation, Investigation, Writing – original draft. **Alberto Carpinteri:** Writing – review & editing, Validation, Supervision.

Declaration of Competing Interest

The authors declare that they have no known competing financial interests or personal relationships that could have appeared to influence the work reported in this paper.

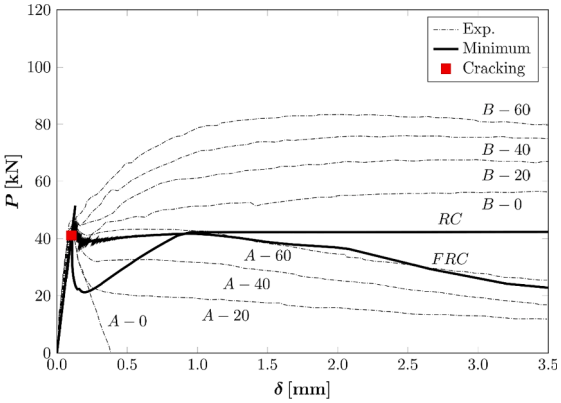

Fig. 12. Prediction of the minimum reinforcement conditions.

Data availability

Data will be made available on request.

References

[1] Alberti MG, Enfedaque A, Gàlvez JC. On the mechanical properties and fracture behaviour of polyolefin fiber-reinforced self-compacting concrete. Constr Build Mater 2014;55:274–88. https://doi.org/10.1016/j.conbuildmat.2014.01.024.
[2] Alberti MG, Enfedaque A, Gàlvez JC, Cànovas MF, Osorio IR. Polyolefin fiber-reinforced concrete enhanced with steel-hooked fibers in low proportions. Mater Des 2014;60:57–65. https://doi.org/10.1016/j.matdes.2014.03.050.
[3] Almusallam T, Ibrahim SM, Al-Salloum Y, Abadel A, Abbas H. Analytical and experimental investigations on the fracture behaviour of hybrid fiber reinforced concrete. Cem Concr Compos 2016;74:201–17. https://doi.org/10.1016/j.cemconcomp.2016.10.002.
[4] Barr BIG, Lee MK, de Place Hansen EJ, Dupont D, Erdem E, Schaerlaekens S, et al. Round-robin analysis of the RILEM TC 162-TDF beam-bending test: Part 1—Test method evaluation. Mat Struct 2003;36(9):609–20.
[5] Barros JAO, Cruz JS. Fracture Energy of Steel Fiber-Reinforced Concrete. Mech of Adv Mat & Structures 2001;8(1):29–45.
[6] Barros JOA, Cunha VMCF, Ribeiro AF, Antunes JAB. Post-cracking behaviour of steel fibre reinforced concrete. Mater Struct 2005;38(1):47–56. https://doi.org/10.1007/BF02480574.
[7] Bencardino F, Rizzuti L, Spadea G, Swamy RN. Experimental evaluation of fiber reinforced concrete fracture properties. Compos B Engng 2010;41(1):17–24.
[8] Fantilli AP, Chiaia B, Gorino A. Fiber volume fraction and ductility Index of concrete beams. Cem Concr Compos 2016;65:139–49. https://doi.org/10.1016/j.cemconcomp.2015.10.019.
[9] Mobasher B, Bakhshi M, Barsby C. Backcalculation of residual tensile strength of regular and high performance fiber reinforced concrete from flexural tests. Constr Build Mater 2014;70:243–53. https://doi.org/10.1016/j.conbuildmat.2014.07.037.
[10] Volpatti G, Martinez JA, Diaz JC, Zampini D. Advanced closed-form moment-curvature formulation for steel fiber-reinforced concrete members. Compos Struct 2022;279:114755. https://doi.org/10.1016/j.compstruct.2021.114755.
[11] Soetens T, Matthys S. Different methods to model the post-cracking behaviour of hooked-end steel fibre reinforced concrete. Constr Build Mater 2014;73:458–71. https://doi.org/10.1016/j.conbuildmat.2014.09.093.
[12] Altun F, Haktanir T, Ari K. Effect of steel fiber addition on mechanical properties of concrete and RC beams. Constr Build Mater 2007;21(3):654–61. https://doi.org/10.1016/j.conbuildmat.2005.12.006.
[13] Barros JOA, Taheri M, Salehian H. A model to simulate the moment-rotation and crack width of FRC members reinforced with longitudinal bars. Engng Struct 2015;100:43–56. https://doi.org/10.1016/j.engstruct.2015.05.036.
[14] Biolzi L, Cattaneo S. Response of steel fiber reinforced high strength concrete beams: Experiments and code predictions. Cem Concr Compos 2017;77:1–13. https://doi.org/10.1016/j.cemconcomp.2016.12.002.
[15] Chunxiang Q, Parnaikuni I. Properties of high-strength steel fiber-reinforced concrete beams in bending. Cem Concr Compos 1999;21(1):73–81. https://doi.org/10.1016/S0958-9465(98)00040-7.
[16] Gorino A, Fantilli AP. Scaled approach to designing the minimum hybrid reinforcement of concrete beams. Materials 2020;13(22):5166. https://doi.org/10.3390/ma13225166.
[17] Holschemacher K, Mueller T, Ribakov Y. Effect of steel fibres on mechanical properties of high-strength concrete. Mater Des 2010;31(5):2604–15. https://doi.org/10.1016/j.matdes.2009.11.025.
[18] Meda A, Minelli F, Plizzari GA. Flexural behaviour of RC beams in fibre reinforced concrete. Compos B Engng 2012;43(8):2930–7.
[19] Mobasher B, Yao Y, Soranakom C. Analytical solutions for flexural design of hybrid steel fiber reinforced concrete beams. Engng Struct 2015;100:164–77. https://doi.org/10.1016/j.engstruct.2015.06.006.
[20] Ning X, Ding Y, Zhang F, Zhang Y. Experimental study and prediction model for flexural behavior of reinforced SCC beam containing steel fibers. Constr Build Mater 2015;93:644–53. https://doi.org/10.1016/j.conbuildmat.2015.06.024.
[21] Vandewalle L. Cracking behaviour of concrete beams reinforced with a combination of ordinary reinforcement and steel fibres. Mater Struct 2000;33(3):164–70. https://doi.org/10.1007/BF02479410.
[22] Dancygier AN, Savir Z. Flexural behavior of HSFRC with low reinforcement ratios. Engng Struct 2006;28:1503–12. https://doi.org/10.1016/j.engstruct.2006.02.005.
[23] Aydin S. Effects of fiber strength on fracture characteristics of normal and high strength concrete. Periodica Polytechnica Civil Engineering 2013;57(2):191–200. https://doi.org/10.3311/PPci.7174.
[24] Choi W-C, Jung K-Y, Jang S-J, Yun H-D. The influence of steel fiber tensile strengths and aspect ratios on the fracture properties of high-strength concrete. Materials 2019;12(13):2105. https://doi.org/10.3390/ma12132105.
[25] Sahin Y, Koksal F. The influences of matrix and steel fibre tensile strengths on the fracture energy of high-strength concrete. Constr Build Mater 2011;25(4):1801–6. https://doi.org/10.1016/j.conbuildmat.2010.11.084.
[26] Yoo D-Y, Yoon Y-S, Banthia N. Flexural response of steel-fibre-reinforced concrete beams: Effects of strength fiber content, and strain-rate. Cem Concr Compos 2015;64:84–92. https://doi.org/10.1016/j.cemconcomp.2015.10.001.

[27] Flàdr J, Bily P. Specimen size effect on compressive and flexural strength of high-strength fibre-reinforced concrete containing coarse aggregate. Compos B 2018;138:77–86. https://doi.org/10.1016/j.compositesb.2017.11.032.
[28] Jones PA, Austin SA, Robins PJ. Predicting the flexural load-deflection response of steel fibre reinforced concrete from strain, crack-width, fibre pull-out and distribution data. Mater Struct 2008;41(3):449–63. https://doi.org/10.1617/s11527-007-9327-9.
[29] Paschalis SA, Lampropoulos AP. Size effect on the flexural performance of ultra high performance fiber reinforced concrete (UHPFRC). In: Proceedings of the 7th RILEM workshop on High Performance Fiber Reinforced Cement Composites (HPFRCC-7), Stuttgart, 2015, pp. 177-184.
[30] Yoo D-Y, Banthia N, Yang J-M, Yoon Y-S. Size effect in normal- and high-strength amorphous metallic and steel fiber reinforced concrete beams. Constr Build Mater 2016;121:676–85.
[31] Lo Monte F, Ferrara L. Tensile behaviour identification in Ultra-High Performance Fibre Reinforced Cementitious Composites: indirect tension tests and back analysis of flexural test results. Mater Struct 2020;53(6).
[32] FIB – Federation International du Bèton, Model Code 2010-Final Draft, Vol. 1, Switzerland, Lausanne, 2012, FIB Bulletin, 65.
[33] RILEM TC 162-TDF, "Test and design method for steel fibre reinforce concrete. Design of steel fibre reinforced concrete using the σ-w method: principles and applications, Mater Struct 2002; 35(5):262-78, DOI: 10.1007/BF02482132.
[34] RILEM TC 162-TDF, Test and design method for steel fibre reinforce concrete. Bending test. Final recommendation, Mater Struct 2002;35(9):579-82, DOI: 10.1007/BF02483127.
[35] RILEM TC 162-TDF, Test and design method for steel fibre reinforce concrete. σ-ε design method. Final recommendation, Mater Struct 2003;36(8):560-67, DOI: 10.1007/BF02480834.
[36] Enfedaque A, Alberti MG, Gàlvez JC, Cabanas P. Numerical simulation of the fracture behaviour of high-performance fibre reinforced concrete by using a cohesive-crack-based inverse analysis, in press.
[37] Lee S-C, Kim H-B, Joh C. Inverse analysis of UHPFRC beams with a notch to evaluate tensile behavior. Adv Mater Sci Engng 2017;2017:1–10.
[38] Löfgren I, Stang H, Olesen JF. Fracture properties of FRC determined through inverse analysis of wedge spitting and three-point bending tests. J Adv Concr Technol 2005;3(3):423–34. https://doi.org/10.3151/jact.3.423.
[39] Carpinteri A. A fracture mechanics model for reinforced concrete collapse. In: Proceedings of the IABSE colloquium on advanced mechanics of reinforced concrete; 1981. p. 17–30.
[40] Carpinteri A. Stability of fracturing process in RC beams. J Struct Engng, ASCE 1984;110(3):544–58. https://doi.org/10.1061/(ASCE)0733-9445(1984)110:3(544).
[41] Carpinteri A, Carpinteri An. Hysteretic behavior of RC beams. J Struct Eng 1984;110(9):2073–84.
[42] Bosco C, Carpinteri A. Discontinuous constitutive response of brittle matrix fibrous composites. J Mech Phys Solids 1995;43(2):261–74. https://doi.org/10.1016/0022-5096(94)00058-D.
[43] Carpinteri A, Massabò R. Bridged versus cohesive crack in the flexural behavior of brittle-matrix composites. Int J Fract 1996;81(2):125–45. https://doi.org/10.1007/BF00033178.
[44] Carpinteri A, Massabò R. Continuous vs discontinuous bridged crack model of fiber-reinforced materials in Flexure. Int J Solids Struct 1997;34(18):2321–38. https://doi.org/10.1016/S0020-7683(96)00129-1.
[45] Carpinteri A, Massabò R. Reversal in failure scaling transition of fibrous composites. J Engng Mech, ASCE 1997;123(2):107–14. https://doi.org/10.1061/(ASCE)0733-9399(1997)123:2(107).
[46] Carpinteri A, Puzzi S. The bridged crack model for the analysis of brittle matrix fibrous composites under repeated bending loading. J Appl Mech, ASME Transactions 2007;74(6):1239–46. https://doi.org/10.1115/1.2744042.
[47] Carpinteri A, Accornero F. The bridged crack model with multiple fibers: Local Instabilities, scale effects, plastic shake-down, and hysteresis. Theor Appl Fract Mech 2019;104:102351. https://doi.org/10.1016/j.tafmec.2019.102351.
[48] Carpinteri A, Accornero F. Residual crack opening in fiber-reinforced structural elements subjected to cyclic loading. Strength Fract Complexity 2020;12(2–4):63–74.
[49] Accornero F, Rubino A, Carpinteri A. Ductile-to-brittle transition in fiber-reinforced concrete beams: Scale and fiber volume fraction effects. Mater Des Process Commun 2020:1–11. https://doi.org/10.1002/mdp2.127.
[50] Rubino A, Accornero F, Carpinteri A. Post-cracking structural behaviour in FRC beams: Scale effects and minimum fibre volume fraction. In: Proceedings of the 2021 fib Symposium of Concrete Structures: New Trends for Eco-Efficiency and Performance, Lisbon, Portugal, 2021, p. 622-31.
[51] Accornero F, Rubino A, Carpinteri A. Post-cracking regimes in the flexural behaviour of fibre-reinforced concrete beams. Int J Solids Struct 2022;248:111637.
[52] Carpinteri A, Accornero F, Rubino A. Scale effects in the post-cracking behaviour of fibre-reinforced concrete beams, Int J Fracture, In press.
[53] Accornero F, Rubino A, Carpinteri A. Ultra-low cycle fatigue (ULCF) in fibre-reinforced concrete beams. Theor Appl Fract Mech 2022;120:103392.
[54] Robins P, Austin S, Jones P. Spatial distribution of steel fibres in sprayed and cast concrete. Mag Concr Res 2003;55(3):225–35. https://doi.org/10.1680/MACR.2003.55.3.225.
[55] Jenq YS, Shah SP. Crack propagation in fiber-reinforced concrete. J Struct Engng, ASCE 1986;112(1):19–34. https://doi.org/10.1061/(ASCE)0733-9445(1986)112:1(19).
[56] Ruiz G, Elices M, Planas J. Size effects and bond-slip dependence of lightly reinforced concrete beams. Eur Struct Integrity Soc 1999;24:67–97. https://doi.org/10.1016/S1566-1369(99)80062-4.
[57] Alwan JM, Naaman AE, Guerrero P. Effect of mechanical clamping on the pull-out response of hooked steel fibers embedded in cementitious matrices. Concr Sci Engng 1999;1(1):15–25.
[58] Cunha VMCF, Barros JOA, Sena-Cruz JM. Pullout behavior of steel fibres in self-compacting concrete. J Mater Civ Engng, ASCE 2010;22(1):1–9. https://doi.org/10.1061/(ASCE)MT.1943-5533.0000001.
[59] Robins P, Austin S, Jones P. Pull-out behaviour of hooked steel fibres. Mater Struct 2002;35:434–42. https://doi.org/10.1007/BF02483148.
[60] Abdallah S, Rees DWA. Analysis of pull-out behaviour of straight and hooked End steel fibres. Engineering 2019;11(6):332–41. https://doi.org/10.4236/eng.2019.116025.